Catalysis Science & Technology

Accepted Manuscript

ROYAL SOCIETY OF CHEMISTRY

www.rsc.org/catalysis

Journal Name

COMMUNICATION

Hydrangea-like $NiCo_2S_4$ hollow microsphere as an advanced bifunctional electrocatalyst for aqueous metal/air batteries

Received 00th January 20xx,
Accepted 00th January 20xx

DOI: 10.1039/x0xx00000x

www.rsc.org/

Mengran Wang, Yanqing Lai, Jing Fang, Furong Qin, Zhian Zhang, Jie Li, Kai Zhang *

The hydrangea-like $NiCo_2S_4$ hollow microsphere is proposed as an advanced electrocatalyst for both oxygen reduction reaction and evolution reaction. The $NiCo_2S_4$ loaded air electrode performs a nice discharge performance in aluminium/air battery. Likewise, rechargeable zinc/air battery testing reveals superior discharge voltages and significantly low charge voltage over 60 cycles.

The growing awareness of environmental protection and resource conservation has aroused the development of environmentally friendly electric vehicles, which make metal/air batteries come to be an ideal storage system for high-performance vehicle[1, 2]. Nevertheless, the large scale application of metal/air batteries is limited by its low power density and energy efficiency, which are associated with the sluggish oxygen reactions and high overpotential at the air cathode of the batteries[3]. Air electrode is crucial to the electrochemical performance of metal/air batteries. There are various factors that affect the performance of air electrodes in metal/air batteries. The catalytic efficiency of the oxygen reaction is one of the most important elements.

As mentioned above, oxygen reduction reaction (ORR) and oxygen evolution reaction (OER) have aroused great attention on account of the applications of next energy generation containing fuel cells and metal/air batteries. Although Pt-based electrocatalysts show wonderful ORR catalytic activity, the high cost and inferior OER activity significantly limit its large scale application[4]. Exploiting non-precious metal bi-functional catalysts for both ORR and OER comes to be a development tendency.

The latest advances in the electrocatalysts field focus on using transition metal oxides[5], sulfides[6], nitrides [7,8], perovskite-type oxides[9], and doped carbons[10] as electrocatalysts. The mixed metal oxides and sulfides involving transition metals often exhibit better electrochemical performance to the synergy of transition metal elements compared to single metal oxide or sulfide[11, 12]. It can be observed in literature that partial substitution of Co with low cost and common elements such as Mn and Ni has greatly enhanced the catalytic activity[13, 14]. Namely, the incorporation of other metal can improve the electrocatalytic property of the metal compounds.

Tremendous efforts in exploiting the substituted metal sulfide and oxide nanomaterials have been focused on the methods to construct higher surface area and more electrochemical active sites[15]. Recently, numerous methods including co-precipitation, hydrothermal, electro-deposition have been employed to synthesize Me-O or Me-S with different morphologies, such as tubes[16], flowers[11], nanoplates[17] and some others on carbon substrates[16]. However, to the best of our knowledge, there are just two reports on Ni-Co-S-based bifunctional catalysts, which report two kinds of materials: $NiCo_2S_4$@graphene and $NiCo_2S_4$ sub-micron spheres. Both of them can be used as a bifunctional electrocatalyst for ORR and OER[19,20]. High performance catalysts for ORR are the most important components in air electrode. And the catalysts with good OER performance can act as an advanced bifunctional electrocatalyst for aqueous metal/air batteries, which is on account of the following fundamentals: (1) The $NiCo_2O_4$ is one of the optimized bifunctional catalysts for both ORR and OER attributed to its low cost, pollution-free and inherent activity towards ORR and OER[21]; (2) $NiCo_2S_4$ often exhibits the similar electrochemical properties compared to $NiCo_2O_4$[22]; (3) The sheet-on-sheet structure often shows high reaction interface area[23]; (4) $NiCo_2S_4$ shows a quite excellent durability in the 6M KOH alkaline solution[24]. In other words, $NiCo_2S_4$ can be identified as one of the most suitable catalyst for the alkaline metal/air batteries.

Herein, we report the hydrothermal synthesis of hydrangea-like $NiCo_2S_4$ microsphere and study its electrochemical properties. The morphology of the as-prepared $NiCo_2S_4$ microsphere is exhibited for the first time as far as we know. The structure is a sheet-on-sheet self-assembly microsphere showing enhanced electrocatalytic performance, which exhibits a lowest value of (E_{OER}-E_{ORR}) of 0.69 V. Moreover, the as-prepared NiCo2S4 performs an advanced discharge properties in the application of

School of Metallurgy and Environment, Central South University, 410083 Changsha, China.
** Corresponding author: Kai Zhang.*
Electronic Supplementary Information (ESI) available: [details of any supplementary information available should be included here]. See DOI: 10.1039/x0xx00000x

aluminium/air batteries and a more stable charge-discharge curve over 60 cycles for zinc/air batteries contrasted to the single metal sulfide, which is attributed to its well durability in 6 M KOH, high surface area and admirable ORR and OER activity.

The hydrangea-like $NiCo_2S_4$ hollow microsphere was successfully obtained by a one-step hydrothermal method which uses Ni and Co salt to offer Ni^{2+} and Co^{2+}, thiourea as a source for the production of S anions. Fig. 1(c) shows the scanning electron microscopy (SEM) image of the fabricated $NiCo_2S_4$, in which we can clearly observe the sheet-on-sheet self-assembled microsphere whose shape is just like a blooming hydrangea showed in the inset. The porous framework often exhibits larger surface area which can perform as the reaction interface for the oxygen reaction. Moreover, the porous structure can shorten the route of diffusion of ionic species and allowing high utilization efficiency of active species [25, 26]. This structure can facilitate diffusion of hydroxyl and oxygen reactants through the highly porous framework. It is obviously seen in Fig 1. (d-f) that the $NiCo_2S_4$ exhibits a structure of hollow sphere whose diameter is about 1 μm with a wall thickness of ~40 nm. The hollow polycrystalline structure of the $NiCo_2S_4$ can adsorb more oxygen and offer more reaction interfaces, then can enhance the electrocatalytic properties of $NiCo_2S_4$. Fig. 1(g) represents the high-resolution transmission electron microscopy (HRTEM) image which demonstrates the polycrystalline structure of the nanosheet on the microsphere. Fig. 1(g) indicates the polycrystalline structure of $NiCo_2S_4$, which consists of different small crystal grains. Four primary interplanar distances, 0.12 nm, 0.14 nm, 0.17 nm and 0.18 nm, can be assigned to the (731), (533), (511), (440) crystallographic planes. The polycrystalline structure can be further demonstrated by the XRD spectra in Fig. 1(h), the corresponding structure is a cubic $NiCo_2S_4$ phase [27].

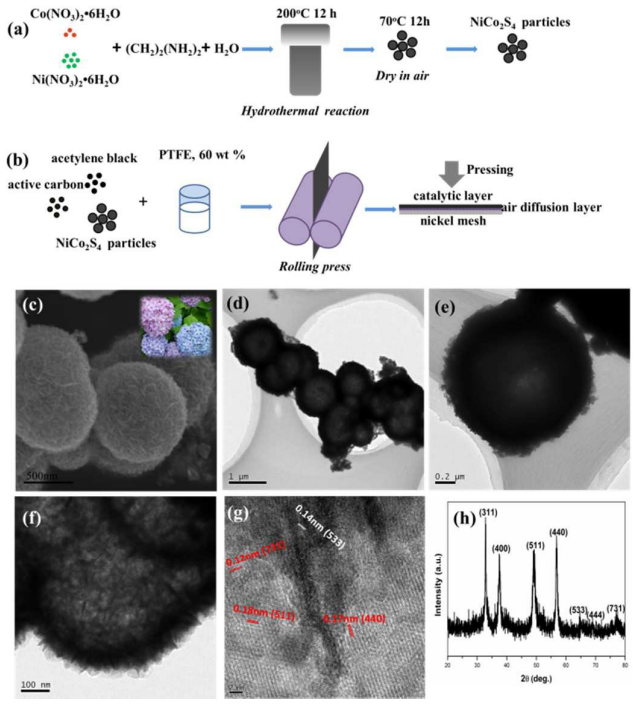

Fig. 1. (a) Schematic illustration of synthesis of $NiCo_2S_4$ catalyst. (b) Schematic illustration of fabrication of air cathode. (c) SEM image (scale bar=500 nm), (d-f) TEM image (scale bar=1 μ m, 0.2 μ m and 100 nm) and (g)HRTEM image (scale bar=2 nm) (h) XRD spectra of $NiCo_2S_4$.

The XPS technique was carried out to better characterize the element valence and components in the hydrangea-like $NiCo_2S_4$ structure. As showed in Fig. 2(a), the Co 2p spectrum can be divided into two spin−orbit doublets and four shake-up satellites, which indicates the coexistence of Co^{2+} and Co^{3+}[24]. One of the two doublets at 778.4 and 793.3 eV, the other at 781.3 and 796.8 eV could be classified into Co^{3+} and Co^{2+}, which exhibits a 2p level splitting of 15.1 and 15.5 eV[28]. Fig. 2(b) shows the Ni 2p spectrum, the peaks at 852.9 eV and 854.4 eV stand for Ni^{2+} and Ni^{3+}, which confirm the existence of different valences of mixed metal[29,30]. The S 2p spectrum can be contributed into two main peaks and two shake-up satellite[12,20]. The results of XPS show that the as-prepared sample has a component of Co^{2+}, Co^{3+}, Ni^{2+}, Ni^{3+} and S^{2-},which is correspond to the $NiCo_2S_4$. The accurate atom ratio of the as-prepared sample is Ni:Co:S=1:2.18:4.07 which is proved by EDS (Fig.1 in ESI).

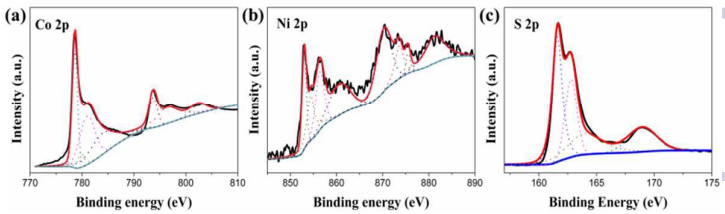

Fig. 2. XPS spectra of (a) Co 2p, (b) Ni 2p and (c) S 2p

The porous texture of the $NiCo_2S_4$ samples above is also studied by N_2 adsorption–desorption isotherms (Fig. 3). This conclusion is fully supported by the pore size distribution (PSD) curves obtained from the N_2 isotherms based on density functional theory (DFT) calculation. The BET specific area is 18.76 m^2 g^{-1} and the predominant pore size is around 4.5 nm and 30 nm. The surface area is quite high for pure sulfides. It offers us an evidence to support the high electrocatalytic activity of the sample. The shape of the isotherm curve indicates the weak interaction of the sample with N_2.

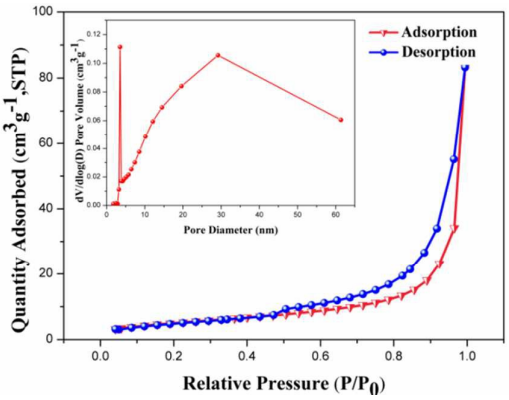

Fig. 3. N_2 adsorption–desorption isotherms of $NiCo_2S_4$ nanostructures and the inset is the image of pore size distribution.

The electrical conductivities of Co_3S_4, NiS and $NiCo_2S_4$ are studied using a four-point probe conductivity measurement. The mixed transition metal sulfide contains different metal ions of two valences can slightly enhance the electric conductivity which can be deduced by the lower sheet resistance of $NiCo_2S_4$ loaded membrane (Table.1 in ESI). In the ORR process, the existence of Ni cation not only effectively activate Co cation, but also enables the oxygen molecules to easily permeate and adsorb onto the pore network of the nanoparticles through electrostatic interaction, leading to a highly efficient ORR reaction [30, 31]. All these facts indicate that the mixed-valent $NiCo_2S_4$ compound can lead to high catalytic activity.

As shown in Fig. 4(a), a high ORR onset potential and low OER onset potential in alkaline solution of the hydrangea-like $NiCo_2S_4$ hollow microsphere can be observed, which leads to a wider application in rechargeable devices. These three sulfides present superior OER catalytic activities. As it is showed in Fig. 4(b), the $NiCo_2S_4$ exhibits the lowest value of (E_{OER}-E_{ORR}) compared to single sulfide and $NiCo_2O_4$ (Fig.2 in ESI). Namely, it shows enhanced ORR and OER activities compared to $NiCo_2O_4$, which proves the great potential of its application in recyclable metal/air batteries, such as rechargeable zinc/air batteries.

This catalyst with a unique porous structure favors efficient electrolyte penetration, oxygen transport, which results in nice electrochemical performance in aqueous metal/air battery. It can be obviously seen in Fig. 4(c) that the $NiCo_2S_4$ loaded air electrode possesses slightly better discharge performance in the application of aluminium/air batteries at a current density of 50 mA cm^{-2} compared to the single catalyst. In addition, the discharge curves of $NiCo_2S_4$ express a quite steady trend. Namely, the $NiCo_2S_4$ shows better durability in 6M KOH which can lead to a stable performance for alkaline aqueous metal/air batteries. Fig. 4(d) demonstrates that the voltage of the aluminium/air batteries goes down with enlargement of current density. The polarization of the air cathode turned to be more serious with the increase of current density, which contributes to the decrease of voltage. Furthermore, the voltage of aluminium/air with $NiCo_2S_4$ possesses higher voltage at most current densities. But the voltage of the Co_3S_4 loaded battery is even higher than $NiCo_2S_4$ loaded battery at some current densities. The possible reason for this experimental phenomenon is that the dominant factor which influences the battery performance is not the catalytic activity of the catalyst at some current densities. Since aluminium anode can offer a fast electrode reaction, the oxygen reduction reaction of the air cathode comes to be the control process for the discharge performance of aluminium/air batteries.

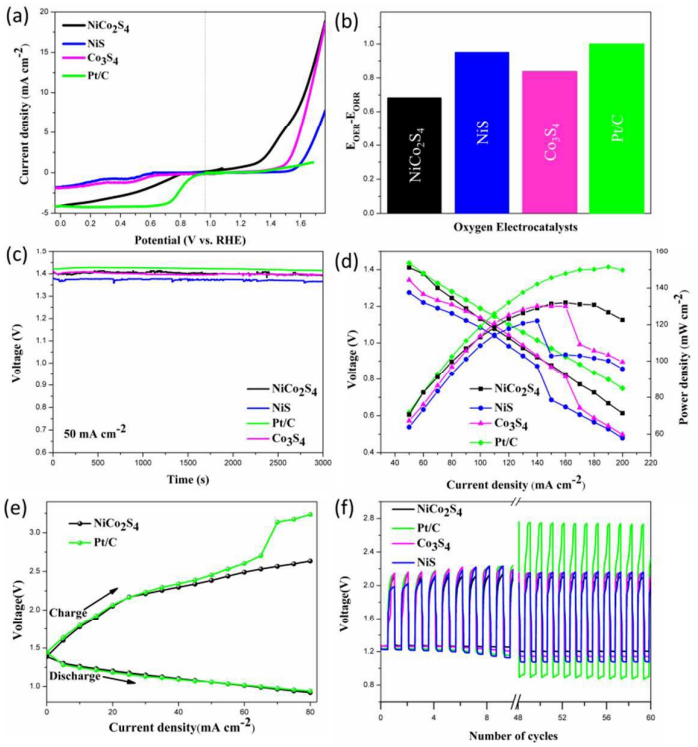

Fig. 4. (a) ORR and OER curves of $NiCo_2S_4$, NiS, Co_3S_4 and Pt/C in O_2-saturated 0.1 M KOH with a sweep rate of 5 mV s−1 at 1600 rpm;(b)The (E_{OER}-E_{ORR}) of four electrocatalysts; (c) Discharge curves of aluminium/air batteries with different catalysts ($NiCo_2S_4$, NiS, Co_3S_4 and Pt/C) at a current density of 50 mA cm^{-2}; (d) Discharge voltages and power densities of aluminium/air batteries with different catalysts at different current densities; (e) Rechargeable zinc/air battery galvanodynamic charge and discharge voltage profiles, and (f) Galvanostatic cycling performance of zinc/air battery obtained at current density of 10 mA cm^{-2} of different catalysts.

To better evaluate practical usage of $NiCo_2S_4$ bifunctional catalyst, it is adopted as the air cathode material for a rechargeable zinc–air battery, which uses oxygen in atmospheric air as the main source of fuel instead of pure oxygen. Galvanodynamically charging and discharging the battery up to 80 mA cm^{-2} result in voltage profiles with sufficiently high performance, confirming effectiveness of the $NiCo_2S_4$ as a bifunctional catalyst (Fig. 4e). Compared to the charge and discharge data of Pt/C catalyst, the as-prepared catalyst shows slightly lower open circuit potential of 1.39 V. Nevertheless, the $NiCo_2S_4$ performs a comparable discharge property with Pt/C at higher current densities, due to its superior rate capability. In terms of charging, lower OER overpotential of the hybrid results in far superior charge voltages at all current densities tested. In addition to the excellent charge and discharge capabilities, the hybrid catalyst demonstrates very stable electrochemical durability in terms of both charge and discharge voltages (1.2 and 2.1 V, respectively) upon galvanostatic cycling up to 60 cycles at 10 mA cm^{-2} with few virtually voltage losses (Fig. 4f). Moreover, notwithstanding does Pt/C demonstrate quite high discharge voltage of 1.25 V for the first three cycles, both charge and

discharge voltages degrade significantly over cycling, leading to poor energy efficiency. The steady voltages acquired with $NiCo_2S_4$ is accounted to high ORR and OER activities, which greatly decreases the overpotentials associated with these reactions thereby avoiding catalyst degradation and subsequent deactivation of the air electrode.

Conclusions

In conclusion, the hydrangea-like $NiCo_2S_4$ microsphere was successfully synthesized by a one-step hydrothermal method, and it can be evaluated as an advanced electrocatalyst for aqueous metal/air batteries. The $NiCo_2S_4$ exhibits an excellent electrocatalytic activity for both ORR and OER in alkaline electrolyte. It shows nice electrocatalytic activity, excellent stability in alkaline electrolyte which makes it an ideal catalyst for aqueous aluminium/air and rechargeable zinc/air batteries. Furthermore, the hydrangea-like structure offers many adsorbed and desorbed sites for oxygen and much reaction interface for reduction and evolution, which possesses great possibilities to develop mixed metal sulfide composition in the application of fuel cell, especially metal/air batteries.

Acknowledgements

The authors acknowledge the financial support of the China Postdoctoral Science Foundation funded project (2015M570686) and National Natural Science Foundation of China (Grant no. 51404304 and 51574288), Natural Science Foundation of Hunan Province (14JJ2001). The authors also thank the Fundamental Research Funds for the Central Universities of Central South University (2015zzts186) and other supports from the Engineering Research Centre of Advanced Battery Materials, the Ministry of Education, China.

Notes and references

1. M. Nestoridi, D. Pletcher, R. J. K. Wood, S. Wang, R. L. Jones, K. R. Stokes and I. Wilcock, Journal of Power Sources, 2008, **178**, 445.
2. A. Kraytsberg and Y. Ein-Eli, Nano Energy, 2013, 2, 468-480.
3. Z. Chen, A. Yu, D. Higgins, H. Li, H. Wang and Z. Chen, Nano letters, 2012, **12**, 1946.
4. G. Wu, K. L. More, C. M. Johnston and P. Zelenay, Science, 2011, **332**, 443.
5. C. Wei, L. Yu, C. Cui, J. Lin, C. Wei, N. Mathews, F. Huo, T. Sritharan and Z. Xu, Chemical communications, 2014, **50**, 7885.
6. D. Geng, N.-N. Ding, T. S. A. Hor, S. W. Chien, Z. Liu and Y. Zong, RSC Adv., 2015, **5**, 7280.
7. K. Zhang, L. Zhang, X. Chen, X. He, X. Wang, S. Dong, L. Gu, Z. Liu, C. Huang and G. Cui, ACS applied materials & interfaces, 2013, **5**, 3677.
8. K. Zhang, L. Zhang, X. Chen, X. He, X. Wang, S. Dong, P. Han, C. Zhang, S. Wang, L. Gu and G. Cui, The Journal of Physical Chemistry C, 2013, **117**, 858.
9. D. Chen, C. Chen, Z. Zhang, Z. M. Baiyee, F. Ciucci and Z. Shao, ACS applied materials & interfaces, 2015, **7**, 8562.
10. L. Dai, Y. Xue, L. Qu, H. J. Choi and J. B. Baek, Chemical reviews, 2015, **115**, 4823.
11. L. Li, Y. Cheah, Y. Ko, P. Teh, G. Wee, C. Wong, S. Peng and M. Srinivasan, Journal of Materials Chemistry A, 2013, **1**, 10935.
12. H. Chen, J. Jiang, L. Zhang, H. Wan, T. Qi and D. Xia, Nanoscale, 2013, **5**, 8879.
13. G. Zhang, B. Y. Xia, X. Wang and X. W. David Lou, Advanced materials, 2014, **26**, 2408.
14. M. Prabu, P. Ramakrishnan and S. Shanmugam, Electrochemistry Communications, 2014, **41**, 59.
15. C. Wei, L. Yu, C. Cui, J. Lin, C. Wei, N. Mathews, F. Huo, T. Sritharan and Z. Xu, Chemical communications, 2014, **50**, 7885.
16. P. Song, Y. Zhang, J. Pan, L. Zhuang and W. Xu, Chemical communications, 2015, **51**, 1972.
17. L. Hu, L. Wu, M. Liao, X. Hu and X. Fang, Advanced Functional Materials, 2012, **22**, 998.
18. Y. Liang, Y. Li, H. Wang, J. Zhou, J. Wang, T. Regier and H. Dai, Nature materials, 2011, **10**, 780.
19. Q. Liu, J. Jin and J. Zhang, ACS applied materials & interfaces, 2013, **5**, 5002.
20. Z. Zhang, X. Wang, G. Cui, A. Zhang, X. Zhou, H. Xu and L. Gu, Nanoscale, 2014, **6**, 3540.
21. Y. Li, L. Zou, J. Li, K. Guo, X. Dong, X. Li, X. Xue, H. Zhang and H. Yang, Electrochimica Acta, 2014, 129, 14.
22. Y. Zhu, Z. Wu, M. Jing, X. Yang, W. Song and X. Ji, Journal of Power Sources, 2015, **273**, 584.
23. S. Q. Chen and Y. Wang, Journal of Materials Chemistry, 2010, **20**, 9735.
24. C. Yuan, J. Li, L. Hou, X. Zhang, L. Shen and X. W. D. Lou, Advanced Functional Materials, 2012, **22**, 4592.
25. T.Y. Ma, S. Dai, M. Jaroniec, S.Z. Qiao, Journal of the American Chemical Society, 2014, **136**, 13925.
26. D. Yu, L. Wei, W. Jiang, H. Wang, B. Sun, Q. Zhang, K. Goh, R. Si, Y. Chen, Nanoscale, 2013, **5**, 3457.
27. S. Peng, L. Li, C. Li, H. Tan, R. Cai, H. Yu, S. Mhaisalkar, M. Srinivasan, S. Ramakrishna and Q. Yan, Chemical communications, 2013, **49**, 10178.
28. D. U. Lee, B. J. Kim and Z. Chen, Journal of Materials Chemistry A, 2013, **1**, 4754.
29. J. Li, S. Xiong, Y. Liu, Z. Ju and Y. Qian, ACS applied materials & interfaces, 2013, **5**, 981.
30. J. Xiao, L. Wan, S. Yang, F. Xiao and S. Wang, Nano letters, 2014, **14**, 831.
31. Y. Gou, X. Liang and B. H. Chen, J. Alloys Compd., 2013, **574**,181.
32. Y. Y. Liang, Y. G. Li, H. L. Wang and H. J. Dai, J. Am. Chem.Soc., 2013, **135**, 2013.